Design and investigation of surface addressable photonic crystal cavity confined band edge modes for quantum photonic devices

P. Nedel,[1] X. Letartre,[1,*] C. Seassal,[1] Alexia Auffèves,[2] L. Ferrier,[1] E. Drouard,[1] A. Rahmani,[3] and P. Viktorovitch[1]

[1]*Université de Lyon, Institut des Nanotechnologies de Lyon INL-UMR 5270, CNRS, Ecole Centrale de Lyon, 36 Avenue Guy de Collongue, F-69134 Ecully Cedex, France*
[2]*Institut Néel, UPR 2940-CNRS, 25 avenue des Martyrs, BP 166, F-38042 Grenoble cedex 9, France*
[3]*Department of Mathematical Science, University of Technology, Sydney, NSW 2007 Australia*
**xavier.letartre@ec-lyon.fr*

Abstract: We propose to use a localized Γ-point slow Bloch mode in a 2D-Photonic Crystal (PC) membrane to realize an efficient surface emitting source. This device can be used as a quantum photonic device, e.g. a single photon source. The physical mechanisms to increase the *Q*/*V* factor and to improve the directivity of the PC microcavity rely on a fine tuning of the geometry in the three directions of space. The PC lateral mirrors are first engineered in order to optimize photons confinement. Then, the effect of a Bragg mirror below the 2DPC membrane is investigated in terms of out-of-plane leakages and far field emission pattern. This photonic heterostructure allows for a strong lateral confinement of photons, with a modal volume of a few $(\lambda/n)^3$ and a Purcell factor up to 80, as calculated by two different numerical methods. We finally discuss the efficiency of the single photon source for different collection set-up.

OCIS codes: (230.5750) Resonators; (270.5580) Quantum electrodynamics; (350.4238) Nanophotonics and photonic crystals.

References and links

1. O. Painter, R. K. Lee, A. Scherer, A. Yariv, J. D. O'Brien, P. D. Dapkus, and I. Kim I, "Two-dimensional photonic band-Gap defect mode laser," Science **284**(5421), 1819–1821 (1999).
2. H. Y. Ryu, H. G. Park, and Y. H. Lee, "Two-dimensional photonic crystal semiconductor lasers: computational design, fabrication, and characterization," IEEE J. Sel. Top. Quantum Electron. **8**(4), 891–908 (2002).
3. D. Englund, D. Fattal, E. Waks, G. Solomon, B. Zhang, T. Nakaoka, Y. Arakawa, Y. Yamamoto, and J. Vucković, "Controlling the spontaneous emission rate of single quantum dots in a two-dimensional photonic crystal," Phys. Rev. Lett. **95**(1), 013904 (2005).
4. T. Asano, B. S. Song, and S. Noda, "Analysis of the experimental Q factors (~ 1 million) of photonic crystal nanocavities," Opt. Express **14**(5), 1996–2002 (2006).
5. Y. Akahane, T. Asano, B. S. Song, and S. Noda, "High-Q photonic nanocavity in a two-dimensional photonic crystal," Nature **425**(6961), 944–947 (2003).
6. F. Bordas, M. J. Steel, C. Seassal, and A. Rahmani, "Confinement of band-edge modes in a photonic crystal slab," Opt. Express **15**(17), 10890–10902 (2007).
7. K. Nozaki, and T. Baba, "Laser characteristics with ultimate-small modal volume in photonic crystal slab point-shift nanolasers," Appl. Phys. Lett. **88**(21), 211101 (2006).
8. M. Toishi, D. Englund, A. Faraon, and J. Vucković, "High-brightness single photon source from a quantum dot in a directional-emission nanocavity," Opt. Express **17**(17), 14618–14626 (2009).
9. J. Claudon, J. Bleuse, N. S. Malik, M. Bazin, P. Jaffrennou, N. Gregersen, C. Sauvan, P. Lalanne, and J. M. Gérard, "A highly efficient single-photon source based on a quantum dot in a photonic nanowire," Nat. Photonics **4**(3), 174–177 (2010).
10. J. Mouette, C. Seassal, X. Letartre, P. Rojo-Romeo, J.-L. Leclercq, P. Regreny, P. Viktorovitch, E. Jalaguier, P. Perreau, and H. Moriceau, "Very low threshold vertical emitting laser operation in InP graphite photonic crystal slab on silicon," Electron. Lett. **39**(6), 526 (2003).

#135924 - $15.00 USD Received 30 Sep 2010; revised 5 Jan 2011; accepted 20 Feb 2011; published 2 Mar 2011

11. S. G. Johnson, J. D. Joannopoulos, and M. Soljačić, "MIT Photonic Bands," *http://ab-initio.mit.edu/wiki/index.php/MIT_Photonic_Bands*.
12. T. Ochiai, and K. Sakoda, "Dispersion relation and optical transmittance of a hexagonal photonic crystal slab," Phys. Rev. B **63**(12), 125107 (2001).
13. L. Ferrier, P. Rojo-Romeo, E. Drouard, X. Letatre, and P. Viktorovitch, "Slow Bloch mode confinement in 2D photonic crystals for surface operating devices," Opt. Express **16**(5), 3136–3145 (2008).
14. J. Mouette, and L. Carrel., "Tessa Project," *http://alioth.debian.org/projects/tessa/*
15. Y. Xu, J. S. Vučković, R. K. Lee, O. J. Painter, A. Scherer, and A. Yariv, "Finite-difference time-domain calculation of spontaneous emission lifetime in a microcavity," J. Opt. Soc. Am. B **16**(3), 465 (1999).
16. B. Ben Bakir, C. Seassal, X. Letartre, P. Viktorovitch, M. Zussy, L. Di Cioccio, and J. M. Fedeli, "Surface-emitting microlaser combining two-dimensional photonic crystal membrane and vertical Bragg mirror," Appl. Phys. Lett. **88**(8), 081113 (2006).
17. P. Viktorovitch, B. Ben Bakir, S. Boutami, J. L. Leclercq, X. Letartre, P. Rojo-Romeo, C. Seassal, M. Zussy, L. Di Cioccio, and J. M. Fedeli, "3D harnessing of light with 2.5D photonic crystals," Laser Photon. Rev. **4**(3), 401–413 (2010).
18. D. Englund, I. Fushman, and J. Vucković, "General recipe for designing photonic crystal cavities," Opt. Express **13**(16), 5961–5975 (2005).
19. D. Ohnishi, T. Okano, M. Imada, and S. Noda, "Room temperature continuous wave operation of a surface-emitting two-dimensional photonic crystal diode laser," Opt. Express **12**(8), 1562–1568 (2004).
20. L. Ferrier, O. El Daif, X. Letartre, P. Rojo Romeo, C. Seassal, R. Mazurczyk, and P. Viktorovitch, "Surface emitting microlaser based on 2D photonic crystal rod lattices," Opt. Express **17**(12), 9780–9788 (2009).
21. N. Tran, S. Combrié, and A. De Rossi, "Directive emission from high-*Q* photonic crystal cavities through band folding," Phys. Rev. B **79**(4), 041101 (2009).
22. R. Esteban, T. V. Teperik, and J. J. Greffet, "Optical patch antennas for single photon emission using surface plasmon resonances," Phys. Rev. Lett. **104**(2), 026802 (2010).
23. X. Letartre, J. Mouette, J. L. Leclercq, P. R. Romeo, C. Seassal, and P. Viktorovitch, "Switching devices with spatial and spectral resolution combining photonic crystal and MOEMS structures," J. Lightwave Technol. **21**(7), 1691–1699 (2003).

1. Introduction

Photonic crystal (PC) nanocavities are promising structures for nanophotonic devices, such as low-threshold lasers [1,2], and single photon sources (SPS) [3]. Due to the unique properties of 2DPC cavity, the size of optical components can be greatly reduced and the strength of light-matter interaction can be significantly increased. The latter is commonly quantified by the Purcell factor (F_p) which is proportional to the ratio between the quality factor (Q) and the modal volume (V) of the microcavity resonant mode. Assuming a dipole source with a perfect spatial and spectral matching with the cavity mode, its spontaneous emission rate is increased by the factor F_p. This effect impacts strongly the efficiency of a SPS which is proportional to the β factor defined by $\beta = \frac{F_p}{F_p + 1}$, β represents the proportion of emitted photons into the optical mode of interest.

The last decade has seen an intense research activity concentrated on the development of new microresonator devices to increase drastically the Q-factor [4–6] and reduce the modal volume [7]. In all the above references, the cavity performance has been improved by carefully adjusting the cavity parameters (e.g. by finely tuning the holes diameters at the vicinity or the resonator) in order to strongly confine the optical mode and to reduce the out-of-plane optical losses.

But the efficiency of a SPS depends also on the directivity of the mode far field pattern, as photons must be collected by an optical component (e.g. a fiber or an optical objective) with a limited numerical aperture. For surface emitting structures, the goal is obviously to get a strongly directional emission pattern. Different designs have been proposed including PC microcavities [8] and micropillars [9]. In the latter, the emission pattern of a vertical nanowire is improved by tailoring the shape of its top end. In the former, the geometry of a very high Q PC microcavity [3] is modified in order to redirect the emission of the mode in the vertical direction.

#135924 - $15.00 USD Received 30 Sep 2010; revised 5 Jan 2011; accepted 20 Feb 2011; published 2 Mar 2011

In this work, we theoretically study the electromagnetic properties of a PC microcavity supporting a Confined slow Bloch Mode (CBM) which is located at the Γ-point in the first Brillouin zone. The choice of this configuration is motivated by two main reasons [10]:

- the k-space localization of the mode is exploited to get directive vertical emitting devices.
- Its small group velocity is used to get a better temporal confinement for a given cavity size

In sections 2 and 3, the geometry of the PC cavity is defined in order to optimize the interaction between a Quantum Dot (QD), such as an InAs/GaAs nanostructure fabricated using the Stransky-Krastanov growth mode, and the resonant mode of interest. Then, in section 4, a Bragg mirror is positioned below the PC resonator to get further control of the out of plane optical losses. In the last section, the far field pattern of the microcavity is studied for different configurations. We propose a figure of merit to describe the efficiency of the nanophotonic cavity that depends on the fraction of photons emitted in the mode of interest, the directivity of the far field pattern and the numerical aperture of the collection system.

2. Design of the basic PC structure

As a basic structure to build a laterally-confined slow light resonator, we use a GaAs-based 2D PC slab that consists of a regular array of air holes, drilled in an air-suspended membrane, and which exhibits a slow light mode around $\lambda = 915nm$. We will first consider a monomode $\lambda/2n$ thick PC slab waveguide, i.e.130nm, the refractive index of GaAs being n = 3.49 at the target wavelength. The first step is to select a slow light mode located in the center of the first Brillouin zone (Γ-point Bloch modes). For that purpose we use the Plane Wave Expansion method (PWE) developed by the MIT [11] to determine the band diagram of the PC structure. It is a well known method in frequency-domain that allows extraction of the Bloch wave functions and frequencies by direct diagonalization.

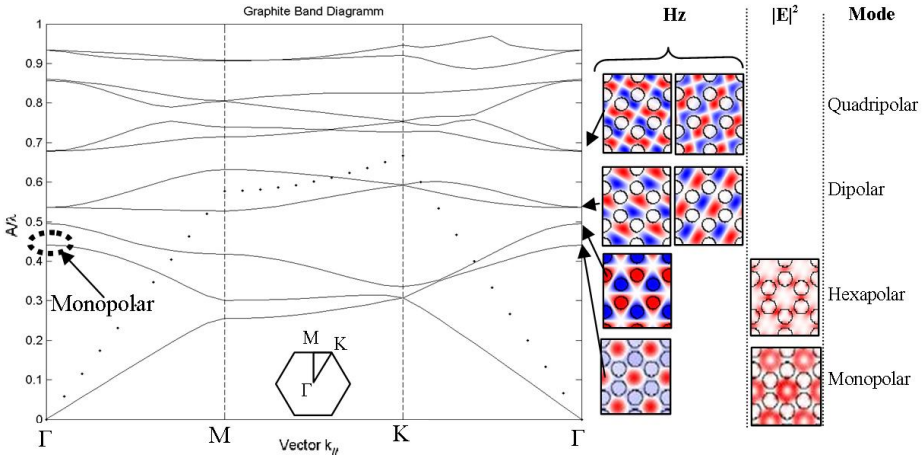

Fig. 1. Band diagram (TE polarization) of the graphite 2D PC (dashed line: light line), z-component of the magnetic field and intensity distributions of several Γ-point modes.

In the remainder of this paper, we will consider a honeycomb (graphite) 2DPC structure for several reasons. (i) Compared to a triangular or a square lattice, the surface filling factor of the semiconductor is higher for a honeycomb structure. QD emitters may then be located far from the holes interfaces, reducing the effect of surface recombination. (ii) The honeycomb structure exhibits several flat bands at the Γ-point [10]. Photons in such modes exhibit a low group velocity and the lateral light confinement is then improved.

#135924 - $15.00 USD Received 30 Sep 2010; revised 5 Jan 2011; accepted 20 Feb 2011; published 2 Mar 2011

Figure 1 shows typical map of the z-component of the magnetic field Hz and electric field intensity map of the different Γ-point band-edge modes. We consider even modes, with respect to a mirror plane located in the centre of the slab. These TE-like modes are suitable for coupling with the fundamental interband transition of InAs/GaAs QDs. To get a large β-factor, we must ensure that the QD emitters couple to only one resonant mode. Accordingly, the Γ-point Bloch mode must be non-degenerate and sufficiently spectrally isolated from the other slow Bloch modes. We see in Fig. 1 that two modes satisfy this requirement: the monopolar and hexapolar modes. The spatial distribution intensity of the monopolar mode is mainly located in the material as compared to the intensity of the hexapolar mode: 82% of the intensity is in the GaAs material. This promotes the interaction of the modes with the emitters. On the other hand, the maximum intensity of the hexapolar mode is close to holes sidewalls in the semiconductor zone of the PC: this mode will therefore couple preferentially to QDs close to the holes surface, which promotes unwanted non-radiative recombination.

A PC lattice parameter A = 420nm is determined so as to operate around λ~915nm. This corresponds to a distance between the closest holes of 240nm.

An air filling factor of *ff* = 37% (defined for the honeycomb structure as $ff = \frac{4\pi}{\sqrt{3}}\left(\frac{r}{A}\right)^2$ where r is the radius of the air holes) is selected. This value results from a balance between 2 criteria. To ensure a good spectral isolation of the monopolar mode with respect to other Γ-point slow Bloch modes, *ff* as high as 50% should be chosen, as it can be shown by calculating band diagrams for different *ff*; however, such a *ff* leads to a separation between closest holes of only 20nm. To keep reasonable technological constraints, we limit *ff* to 37%, which corresponds to a 50 nm separation.

3. Laterally confined Γ-point Bloch mode

For an infinite PC and for a non-degenerate Γ-point Bloch mode, the light is perfectly confined in the PC and doesn't suffer from losses [12], but its lateral extension is theoretically infinite. In order to confine the light within a reduced area, one can locally change the topography of the PC structure, for example the radii of several air holes. We used this photonic heterostructure concept [6,13] to control the modal volume and lateral optical losses, and to increase the Q/V ratio. As the band curvature of the monopolar mode is negative around the Γ-point, the light confinement may be obtained by decreasing the radii of air holes in barrier region: the energy of the barrier band decreases and the photons should stand preferably in the core area, where the holes radii are larger. Such a photonic heterostructure based on the honeycomb structure described above was simulated using the 3D-Finite Difference Time Domain method (FDTD) [14]. The spatial step is λ/(10n)~25nm along each direction. We use a sub-pixel averaging method for the optical index to ensure reproducible and valid simulation results. This is especially required for weak variations of parameters such as radii of air holes inside or outside of the cavity. For all simulations presented in this article, the simulation domain is taken sufficiently large to avoid a direct interaction of the CBM with the surrounding PML (Perfect Match Layer, absorbing boundary conditions). Taking into account these calculation conditions, the main optical sources of losses are not the imperfections due to the spatial meshing but the intrinsic losses mechanism of the CBM.

We consider the PC structure shown in Fig. 2: the whole PC structure contains elementary crystal cells, including a 7-cells core area with fixed holes radii (ff_{core} = 37%). We then simulate five structures, with different lower air hole radii in the cladding region (ff_{clad} = 36, 35, 33, 31 and 29%). For each structure we determine numerically the Q-factor and the modal volume (V_m), in order to calculate F_p. To determine the spectrum of the PC cavity, a dipole source is located inside the middle-plane membrane; a narrow temporal Gaussian pulse is emitted in order to probe the PC structure over a wide spectral range. Figure 3 shows a typical spectrum of the photonic heterostructure, obtained from a Fourier transform of the field at a

#135924 - $15.00 USD Received 30 Sep 2010; revised 5 Jan 2011; accepted 20 Feb 2011; published 2 Mar 2011

specific location in the structure. The resonance peaks are associated to different Γ-point Bloch modes (namely monopolar and hexapolar). For the monopolar mode, harmonics are observed which are due to the lateral confinement.

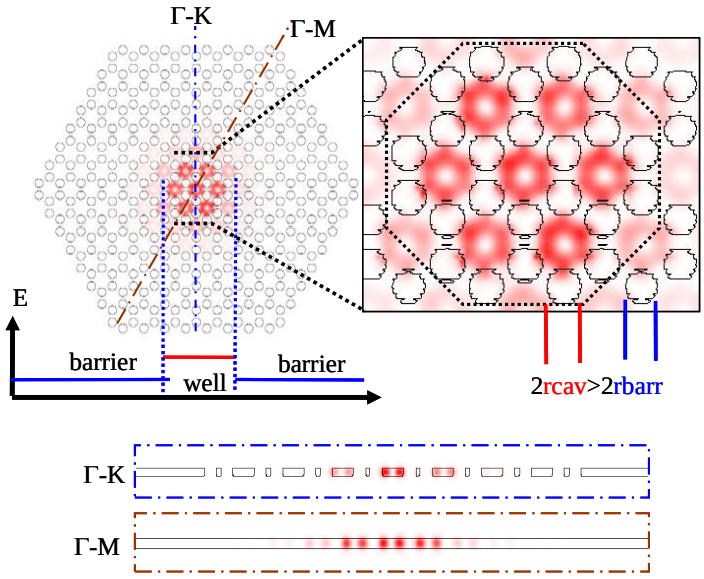

Fig. 2. planar and cross-section views of the electric field intensity map for monopolar mode confined in a photonic heterostructure cavity, ff_{cav} = 37% and ff_{bar} = 31%.

The field map of the fundamental Confined Bloch Mode (CBM) is obtained by exciting the PC structure at the corresponding resonant wavelength (~930nm on Fig. 3). V_m is calculated by integrating the electric energy density over the FDTD simulation workspace:

$$V_m = \iiint \frac{n^2(x,y,z)|\vec{E}|^2}{\max\left[n^2(x,y,z)|\vec{E}|^2\right]} dxdydz.$$

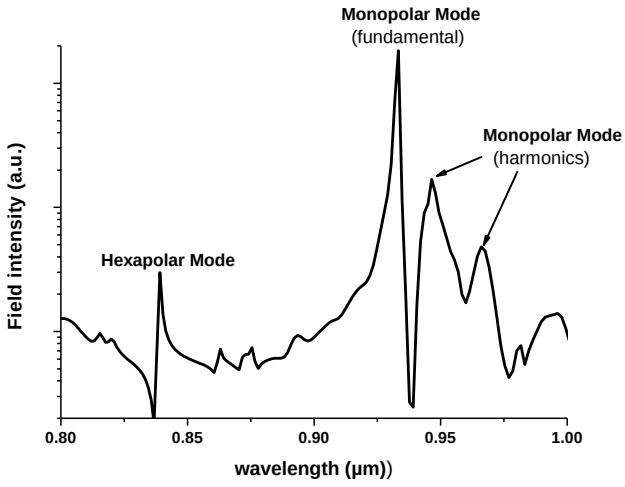

Fig. 3. Typical spectrum of the photonic heterostructure (3D-FDTD simulation).

#135924 - $15.00 USD Received 30 Sep 2010; revised 5 Jan 2011; accepted 20 Feb 2011; published 2 Mar 2011

Then, the Purcell factor F_p is calculated using the well known formula: $F_p = \frac{3}{4\pi^2}\frac{Q}{V_m}\left(\frac{\lambda}{n}\right)^3$, where n is the refractive index of the background material (GaAs in our case).

We have used another method to determine directly the Purcell factor without calculating the modal volume and the quality factor of the mode. It is well known that the Purcell factor can be determined, without recourse to quantum theory, by simply calculating the ratio of the total power emitted by a dipole in resonance with the cavity mode and the emitted power by the same dipole in the homogeneous, un-patterned, background material [15]. The resonant mode is excited with a sinusoidal electromagnetic wave by a classical oscillating dipole (to get a maximum F_p, the dipole must be located at an electric field antinode, and collinearly oriented with respect to the electric field polarization), and we calculate the total flux of Poynting vector through the total area of the workspace. A similar simulation is performed in the case of a dipole in a uniform GaAs material. In this work, both methods have been used and the discrepancy between the obtained Purcell factors is found to be less than 5%.

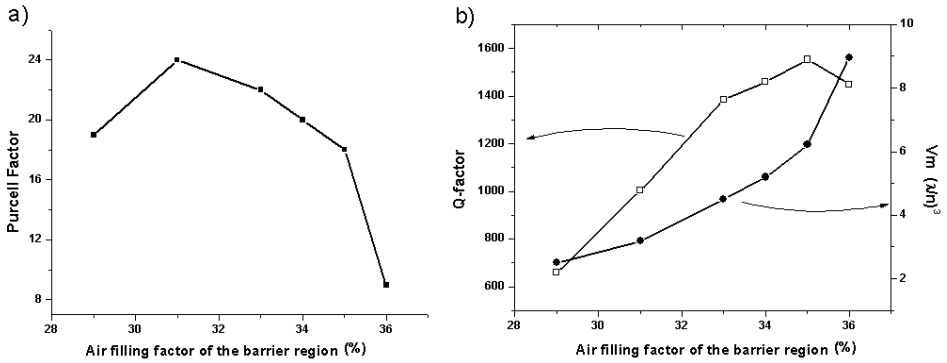

Fig. 4. Evolution of the CBM properties as a function of the barrier filling factor: (a) F_p versus ff_{barr}; (b) Q and V_m versus ff_{barr}.

This way, the *Q*-factor, the mode volume V_m and the resulting Purcell factor are calculated as a function of the barrier filling factor (see Fig. 4(a) and 4(b)). For small ff_{bar}, the *Q* factor increases when the filling factor difference decreases (see Fig. 4(b)), indicating reduced scattering losses at the microcavity boundaries [6]. When ff_{bar} tends to ff_{core}, lateral losses through the barrier become dominant and the *Q*-factor is decreased. The lateral confinement process is well illustrated by the evolution of V_m with $ff_{bar.}$: a large filling factor difference leads to a large photonics "band offset" and then to a better spatial confinement. Finally, a maximum Purcell factor F_p~24 is reached for ff_{bar} = 31%, with *Q*~1000 and $V_m = 3.2(\lambda/n)^3$. For this specific configuration, we have checked that, keeping the same core size, the addition of arrays of air holes in the barrier region does not improve the *Q*-factor, indicating that optical tunneling through the barrier is negligible. This indicates that the main losses are out of plane losses through scattering at the interfaces between the core area of the PC and cladding areas, and within the core area of the PC. It is worthwhile to notice that V_m is significantly smaller than the physical volume of the cavity ($\approx 10(\lambda/n)^3$). This is a clear evidence of the effect of slow group velocity induced lateral confinement, which is combined with the lateral cavity mode confinement.

4. Control of the vertical and lateral losses of the Confined Bloch Mode

For the structure described above, the *Q*-factor is mainly controlled by the coupling between the CBM and the radiative continuum. This coupling can be controlled by an accurate design

#135924 - $15.00 USD Received 30 Sep 2010; revised 5 Jan 2011; accepted 20 Feb 2011; published 2 Mar 2011

of the electromagnetic environment of the PC membrane in the vertical direction. As it has been shown in previous works [13,16], the radiation pattern of a Γ-point CBM is quite directional, such that the use of a Bragg mirror positioned below the PC membrane at a three quarter wavelength distance, can greatly inhibit this coupling by destructive interference, and therefore increase the *Q*-factor.

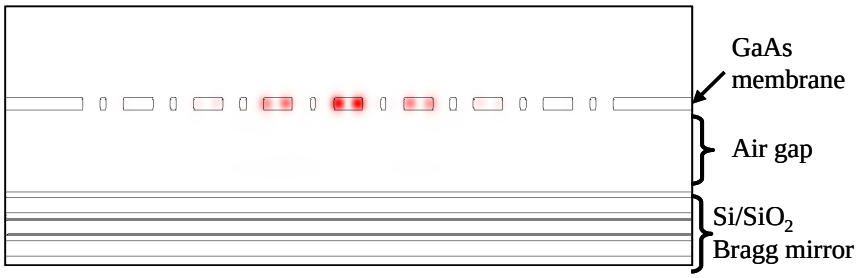

Fig. 5. Cross-section of the electromagnetic field intensity of the CBM, for a PC heterostructure positioned above a Bragg mirror.

The PC structure optimized in the last section (with F_p ~24), is positioned above a Bragg mirror composed by three pairs of $\lambda/4n$ thick Si/SiO_2 layers, with a reflectivity around 98% at 915nm (Fig. 5). The first advantage of this configuration is to direct photons only upwards. Moreover, as it can be shown in Fig. 6(a), the *Q*-factor can be increased to about 2100 (instead of ~1000 without Bragg mirror) for an air gap a_g between the PC membrane and the mirror of about 830nm. In this configuration, we obtain $V_m = 3.6(\lambda/n)^3$, which yields F_p~44.

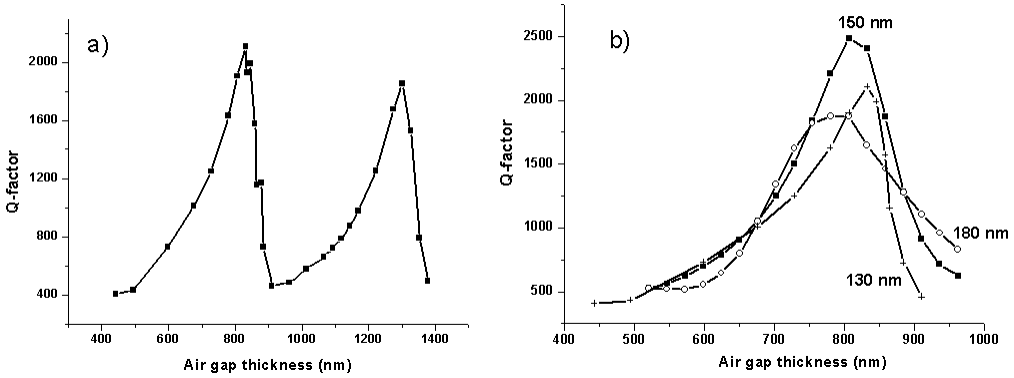

Fig. 6. Evolution of the CBM Q-factor versus air gap thickness: (a) for a 130nm thick membrane, (b) for different thicknesses of the membrane: 130 nm (+), 150 nm (▪), 180 nm (○).

It can be noticed that the mode volume is only 10% larger, as compared to the configuration without mirror, indicating that the spatial confinement of the mode remains good. In fact, this small increase of V_m can be explained by considering that the field is spread across the PC membrane and the air gap located below. To be more precise, it can be shown [17] that the relative part of electromagnetic energy contained into the air gap η_{gap} Eq. (1) is given by the ratio between the times spent by photons respectively in the air gap and in the PC membrane, providing the relation:

$$\eta_{gap} = \frac{\frac{2a_g}{\lambda}}{\frac{2a_g}{\lambda} + \frac{Q_{CBM}}{2\pi}} \qquad (1)$$

#135924 - $15.00 USD Received 30 Sep 2010; revised 5 Jan 2011; accepted 20 Feb 2011; published 2 Mar 2011

where a_g is the optical thickness of the air gap and Q_{CBM} the quality factor obtained without the underlying Bragg mirror. In our case, we find η_{gap}~2%. Considering a PC membrane (resp. an air gap) thickness of 135nm (resp. 830nm), the increase of the effective mode thickness can be estimated to about 10%, in agreement with the value obtained by direct numerical calculation of the modal volume.

Using coupled mode theory (CMT) arguments, and as described in [16], we should get a maximized *Q*-factor for a gap size $e = 690nm$ ($a_g = 3\lambda/4$) and, in Fig. 6(a), the peaks shape should be symmetric (see the appendix). The difference between the 3D-FDTD simulation and the CMT model is explained by two approximations. First, the structure simulated by FDTD is not an infinite and uniform PC excited by a plane wave: the specific design and lateral confinement lead to optical losses that are not fully vertical (see next section). Second, a $\lambda/2$ equivalent optical thickness of the PC structure is considered in the CMT model, which is the optimum case for inhibition of radiative coupling (see the appendix). For the structure simulated by FDTD, a limited part of the resonant mode is located in the air holes and the effective optical thickness is reduced. In order to refine the prediction of the optimum geometry, we performed additional simulations, considering structure with different membrane thickness. Figure 6(b) displays the *Q*-factor dependence on the air-gap thickness, for GaAs membranes with three different thicknesses: 130, 150 and 180nm.

A maximum quality factor *Q*~2500 is found for a 150nm thick membrane, resulting in an increased Purcell factor F_p = 52. Moreover, a quasi symmetric evolution of the *Q*-factor around this maximum is observed. Assuming that this thickness is optically "λ/2", we deduce an average refractive index of 3.05 for the PC membrane. A similar value is obtained by weighting the refractive indices of GaAs and air by the spatial profile of the electromagnetic energy.

This multilayer configuration leads to at least a twofold increase of the *Q*-factor, indicating a strong inhibition of radiative coupling. We can now guess that optical losses may be, to a certain extent, determined by the lateral tunneling through the barrier. To check this hypothesis, we increase the number of rows of graphite unit cell in the barrier region from 5 to 11 (for more than 11 rows the Q remains constant). We achieve a maximum quality factor of *Q*~2950 for the 130nm membrane's thickness; this increase indicates that the lateral losses were not completely inhibited. For a 150nm membrane's thickness (optically "λ/2"), the quality factor finally reaches *Q*~3800 leading to F_p = 80.

5. Far-field pattern of the surface emitting Confined Bloch Mode

The far field diagram (FFD) of the CBM modes are obtained by first calculating the discrete Fourier transform (DFT) of the field components at about 200 nm above the membrane. The DFT is then filtered to remove the near-field components [18];

#135924 - $15.00 USD Received 30 Sep 2010; revised 5 Jan 2011; accepted 20 Feb 2011; published 2 Mar 2011

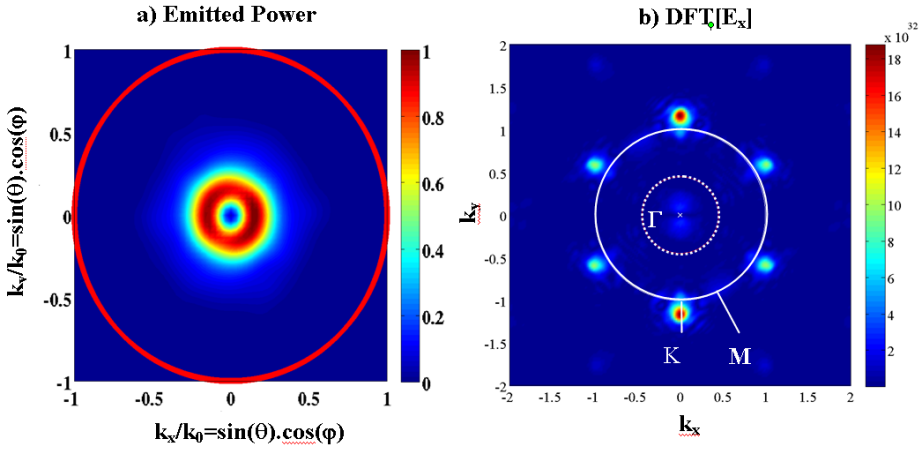

Fig. 7. (a) Far field diagram in k-space for the CBM mode for ff_{cav} = 37%, ff_{bar} = 31% and without Bragg mirror (F_p~24). (b) Fourier transform of the Ex-field map of same mode at 200nm above the membrane - the white dashed line is the light cone and the white circle has a radius of 2π/A, the Γ-point is the center of each circle, K and M points are indicated.

We first applied this method to the case of the resonator without Bragg mirror. The DFT of the Ex field (Fig. 7(b)) shows that the main part of the mode is under the light line, and a remaining part is indicated by two lobes around the Γ-point over the light line. As a consequence, the FFD shown in Fig. 7(a) indicates that out of plane losses are mainly emitted close to the perpendicular direction. As discussed before, for symmetry reasons, no light from the CBM couples to radiation modes exactly at the Γ-point. This doughnut pattern is commonly observed experimentally for localized Γ-point Bloch modes [19,20]. Integration of this far-field pattern indicates that 90% of the light is emitted within a 50° cone. Even if the mode is fairly directive, an important drawback is that the emission occurs both above and below the membrane, therefore only half of the emitted photons, at best, can be collected above the structure.

Positioning the resonator above a Bragg mirror allows for redirecting the emission mostly above the membrane. Therefore, we have calculated the FFD for two different air gap thicknesses between the PC membrane and the Bragg mirror (Fig. 8).

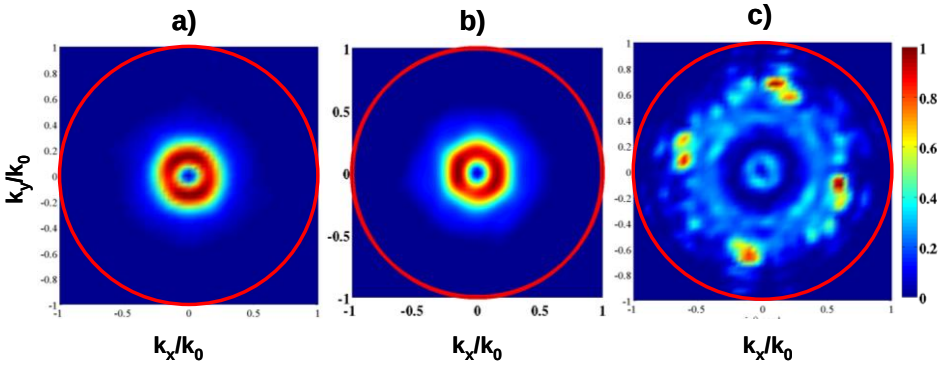

Fig. 8. Far field diagram in k-space of the CBM mode: ff_{cav} = 37%, ff_{bar} = 31% for a membrane's thickness of 150nm (λ/2 optical thickness): (a) without Bragg mirror (F_p ~24); (b) on a Bragg mirror with an air gap for constructive interferences (F_p ~10); c)on a Bragg mirror with an air gap for destructive interferences resulting in a maximized quality factor (F_p~80).

For a distance corresponding to a maximum *Q*-factor (3λ/4 equivalent optical thickness), the losses around the gamma point are inhibited and the relative weight of the losses away

#135924 - $15.00 USD Received 30 Sep 2010; revised 5 Jan 2011; accepted 20 Feb 2011; published 2 Mar 2011

from the vertical direction is then increased, leading to a less directional emission pattern. On the contrary, for a distance corresponding to a minimum Q factor ($\lambda/2$ equivalent optical thickness), the FFD is very similar to those of the CBM without Bragg mirror. More specifically, the function $I(\theta)$, where $I(\theta)\mathrm{d}\theta$ is the emitted power between the cones of angle θ and $\theta + d\theta$, is plotted on Fig. 9 for 3 configurations: the 150nm thick PC membrane (a) without Bragg mirror (F_p~26), (b) with a Bragg mirror located for constructive interference (F_p~10), (c) with a Bragg mirror located for destructive interference (F_p ~80). It can be seen that, with this approach, a trade-off has to be found between the Purcell factor and the directivity of the device.

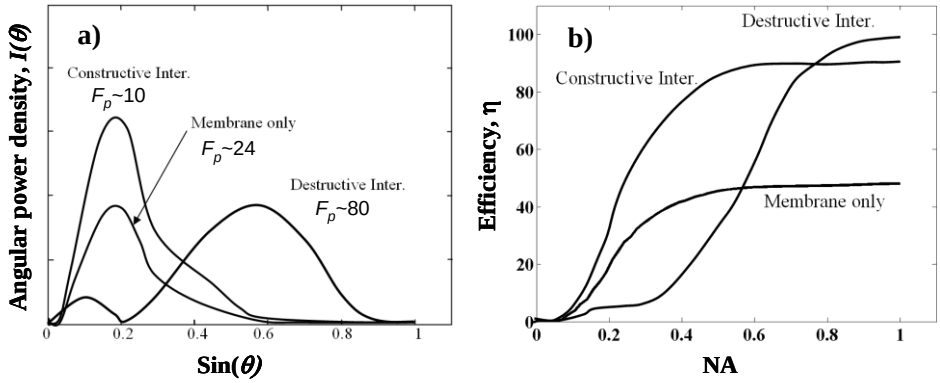

Fig. 9. For the three configurations: (a) Angular emitted power density, $I(\theta)$. (b) Percentage of the collected emitted power as a function of the *NA*.

In order the quantify the efficiency of a SPS, a factor of merit (η) can be defined as the product of the β factor, which corresponds to the fraction of the dipole emission that couples to the mode of interest, by the collection efficiency (γ) of an optical device (e.g. an objective lens) with a numerical aperture *NA*. Then η can be expressed as Eq. (2):

$$\eta = \beta \times \gamma = \frac{F_p}{1+F_p} \times \int_0^{\theta_{NA}} I(\theta)\, d\theta \qquad (2)$$

For the three configurations, the efficiency of the device (η) is plotted as a function of the *NA* of the collection (Fig. 9(b)). We thus see that the optimum configuration will depend heavily on the collection mechanism. For a single-mode optical fiber with a *NA*~0.2, only the solution with Bragg mirror in constructive interference is suitable, achieving a moderate efficiency of about 35%. We expect a better collection with a more sophisticated optical system such as a lensed fiber or a spherical lens with, e.g., a numerical aperture of ~0.95. In this case, a very high efficiency (η~0.99) can be reached with the F_p -optimized structure. This value can be compared with those obtained for different devices proposed in the literature:

- for a PhC microcavity, TRAN et al. [21] get, if considering backward and upward collections, comparable (resp. three time lower) efficiencies for large (resp. small) NA .
- "patch" nano-antennas [22] demonstrate, for *NA* = 0.95, an efficiency of 0.7, instead of 0.99 in our study (case of destructive interferences).
- vertical nanowires [9] exhibit, for *NA* = 0.75, a theoretical efficiency of 0.95, instead of 0.90 in this paper (both for destructive or constructive interferences)

#135924 - $15.00 USD Received 30 Sep 2010; revised 5 Jan 2011; accepted 20 Feb 2011; published 2 Mar 2011

6. Conclusion

In this paper, designs of vertical-emission PC-based active optical nano-devices were proposed. Combining slow group velocity and cavity mode confinement schemes, strong photon confinement is achieved in structures that consist of honeycomb planar PC lattices operating at the Γ-point and dielectric Bragg reflectors. These structures are attractive candidate to build devices like SPS or low threshold nanolasers. Purcell factor of such structures could be predicted by FDTD and with two distinct methodologies, either by calculating Q and Vm, or by direct simulation of the emitted power. Fp up to 80 is expected for the configuration chosen in our investigation. The global efficiency of these photonic nano-devices results from a compromise between photon confinement and emission diagram, and can be maximized provided that an optimized matching of the structure with the photon collection set-up is achieved.

Appendix

In this appendix we calculate analytically the effect of a multilayer system (namely a Bragg mirror) on the optical properties of a Γ-point Bloch mode. For that purpose we use the formalism developed in [23], which associates temporal coupled mode theory and matrix transfer method. Following this phenomenological method, the photonic structure of Fig. 5 is modeled as a multilayer stack embedding a resonant mode in the photonic crystal membrane (PCM) which represents the Γ-point Bloch mode. Neglecting lateral losses, the optical properties of the mode is then fully determined by 2 parameters: its resonant frequency ω_0 and its coupling to vertical plane wave $1/\tau$ ($Q = \omega_0\tau$). Then, the complex resonant frequency of this mode is: $\tilde{\omega}_0 = \omega_0 + \frac{j}{\tau}$. The complex resonant frequency, $\tilde{\omega}$, of the whole structure can then be calculated:

$$\Delta\tilde{\omega} = \tilde{\omega} - \tilde{\omega}_0 = \frac{j}{\tau_c}\left[1 + \frac{\alpha_{PCM}\left(r_u + r_d\right) + 2r_u r_d}{\alpha_{PCM}^2 - r_u r_d}\right] \text{ with } \alpha_{PCM} = e^{i\varphi_{PCM}} \qquad \text{(A1)}$$

r_u and r_d are the reflectivity seen from the PCM at its interface:

$$r_u = \frac{n_{PCM} - 1}{n_{PCM} + 1} \quad r_d = \frac{r_u\alpha_S + r_{bragg}}{\alpha_S + r_u r_{bragg}} \text{ with } \alpha_S = e^{2i\phi_S}$$

n_{PCM} is the effective optical index of the PCM. r_{bragg} is the reflectivity of the Bragg mirror. φ_{PCM} (resp. φ_S) are the dephasing of a vertical plane wave through the PCM (resp. the spacer). They depends on the optical frequency and equation (Eq. (A1)) has to be solved numerically.

Solving equation (Eq. (A1)) for different PCM and spacer optical thicknesses (ℓ_{PCM}, ℓ_S) leads to the following results:

- for a given ℓ_{PCM}, the evolution of the quality factors with ℓ_S exhibits maxima. Only if ℓ_{PCM} is half-wavelength, these peaks are symmetric.
- the maximum quality factor exaltation is obtained if ℓ_{PCM} is half-wavelength and ℓ_S is quarter-wavelength.

Acknowledgement

We would like to acknowledge financial support from the French National Research Agency (ANR) through the PNANO program (IQNONA project). We thank Laurent Carrel for his

#135924 - $15.00 USD Received 30 Sep 2010; revised 5 Jan 2011; accepted 20 Feb 2011; published 2 Mar 2011

assistance in computer modeling. Adel Rahmani acknowledges support under the Merit Allocation Scheme on the NCI National Facility at the ANU.

#135924 - $15.00 USD Received 30 Sep 2010; revised 5 Jan 2011; accepted 20 Feb 2011; published 2 Mar 2011